ORIGINAL SCIENTIFIC PAPER

CROATICA CHEMICA ACTA

Croat. Chem. Acta **2025**, *98*(3), 175–183
Published online: June 28, 2025
DOI: 10.5562/cca4174

HKD 1926

Kinetic and Morphological Study of Zn Electrodeposition onto HOPG from Alkaline Aqueous Solutions

Luis Humberto Mendoza-Huizar

Área Académica de Química. Ciudad del Conocimiento. Universidad Autónoma del Estado de Hidalgo, Carretera Pachuca-Tulancingo km. 4.5, CP. 42184 Mineral de la Reforma, Hidalgo, México
Author's e-mail address: hhuizar@uaeh.edu.mx

RECEIVED: April 4, 2025 * REVISED: May 18, 2025 * ACCEPTED: May 21, 2025

Abstract: In this study, we conducted an electrochemical analysis of the electrodeposition of Zn onto a highly oriented pyrolytic graphite (HOPG) electrode from an aqueous solution containing 0.01 M $ZnSO_4$ and 1 M $(NH_4)_2SO_4$ at pH 8 and 25 °C. Voltammetric studies indicate that, under our experimental conditions, Zn electrodeposition is an irreversible diffusion-controlled process. Potentiostatic study was used to determine kinetic parameters such as the number of active nucleation sites (N_0), and the nucleation rate (A), which exhibited a dependence on the applied potential. The morphology of the Zn deposits was examined using scanning electron microscopy (SEM). The results show that electrodeposition at lower potentials leads to rougher surfaces, likely due to increased hydrogen evolution, which interferes with the uniformity of Zn growth. In contrast, at more positive potentials, Zn deposits appeared more homogeneous, suggesting a more controlled nucleation and growth process with reduced proton reduction process.

Keywords: zinc, electrodeposition, HOPG, kinetic, HER, SEM.

INTRODUCTION

ZINC-based coatings effectively prevent corrosion in materials like steel and iron, making them vital in industries such as automotive, construction, and infrastructure.[1] Beyond anticorrosive uses, zinc coatings show potential in optoelectronics,[2,3] solar cells,[4] sensors,[5] and batteries,[6–12] due to their conductive and protective properties, enhancing device performance and longevity. Specifically, the pH and chemical composition of the electrolyte solution are crucial in determining the final properties of the zinc deposit.[13–15] Acidic baths, commonly used for their high efficiency and faster deposition rates,[12] generally involves hydrogen embrittlement, leading to cracking.[16] Alkaline zinc plating, with higher pH, offers smoother deposition, better ductility, and corrosion resistance.[17–21] However, conventional alkaline baths often use toxic cyanide, creating high wastewater treatment costs.[22–26] This has spurred the search for cyanide-free alternatives, though non-cyanide baths may have lower cathode efficiency or produce poor-quality deposits.[27,28] Efforts are underway to develop non-cyanide alkaline zinc electrolytes with complexing agents to improve plating quality, efficiency, and adhesion.[27–35] On the other hand, the nature of the substrate plays a fundamental role in the electrodeposition of zinc, influencing adhesion, morphology, deposition rate among others.[36–38]

Specifically, the electrodeposition of zinc onto carbon substrates has gained significant attention, particularly in the production of zinc-carbon composites for battery applications.[6–12] However, relatively few studies have investigated the nucleation parameters associated with zinc electrodeposition on carbon substrates,[6,10,16,39–46] from neutral,[6,45] acidic,[39,40,42,46] and alkaline plating baths.[43,44] The available results suggest that zinc electrodeposition on glassy carbon electrodes (GCE) transitions from instantaneous to progressive as the concentration of zinc ions in the bath increases, with the nucleation rate being governed by charge transfer.[46] Also, it was reported an instantaneous

nucleation from acetate baths on GCE, which shifted to progressive nucleation when the applied potential was increased.[45] Similarly, Torrent et al. observed instantaneous nucleation and hemispherical 3D growth on GCE.[39] In contrast, zinc electrodeposition on highly oriented pyrolytic graphite (HOPG) electrodes has been less extensively studied,[6,42,44] and the results suggest a predominance of progressive nucleation. Thus, based on our literature review, there is a notable gap in the determination of the kinetic parameters associated with the nucleation and growth processes of zinc electrodeposition from ammoniacal sulfate baths onto HOPG under alkaline conditions. Therefore, this study aims to address this gap by investigating zinc electrodeposition on HOPG from sulfate solutions under alkaline conditions. Techniques such as cyclic voltammetry, chronoamperometry, and scanning electron microscopy (SEM) are employed to examine the process. The main goal of this work is to explore the kinetics of zinc electrodeposition on HOPG without the use of organic additives, using an electrolyte bath consisting of 0.01 M $ZnSO_4$ and 1 M $(NH_4)_2SO_4$ at pH = 8, to obtain detailed insights into the characteristics of the deposits formed under alkaline conditions.

METHODOLOGY

Zinc electrodeposition on Highly Oriented Pyrolytic Graphite (HOPG) electrodes was carried out using an aqueous solution of 0.01 M $ZnSO_4$ and 1 M $(NH_4)_2SO_4$, maintaining a pH of 8 at a temperature of 25 °C. The pH of the plating solution was adjusted using a 1 M NaOH solution. All solutions were prepared with analytical-grade chemicals and ultrapure water from a Millipore-Q system. Prior to the experiments, the solutions were deoxygenated by bubbling nitrogen gas for 15 minutes. HOPG electrodes (grade ZYA) were supplied by MikroMasch (Watsonville, CA, USA). Freshly cleaved HOPG surfaces with an area of 0.25 cm^2 were used as working electrodes. A graphite bar with a surface area larger than that of the working electrode served as the counter electrode. A saturated calomel electrode (SCE) was used as the reference electrode, and all measured potentials were reported relative to this reference. Electrochemical experiments were conducted using a BAS potentiostat connected to a computer running BAS100W software, which allowed experiment control and data acquisition. To characterize the electrochemical behavior of the electrode in the deposition bath, cyclic voltammetry was performed within a potential range of –0.600 to –1.600 V at scan rates between 10 and 300 mV s^{-1}. The kinetics of zinc deposition on HOPG were investigated under potentiostatic conditions by analyzing current density transients using the potential step method. The perturbation potential started at–0.600 V, with potential steps applied at different values specified in this study. The microstructural features of the deposited layers were examined using a scanning electron microscope (SEM; JEOL 6300).

RESULTS AND DISCUSSION

Voltammetric Study

In all the experiments, the scan started in the zero-current region at –0.6 V in the cathodic direction. Around –1.28 V, a current drop was recorded, associated with the beginning of an electrocrystallization process (E_{cris}). Continuing in the cathodic direction, peak A was observed at –1.32 V. Here, it is important to mention that, at pH = 8, the predominant zinc chemical species is the complex $[Zn(NH_3)_4(H_2O)_2]^{2+}$,[6] and the zinc electrodeposition occurs according to the following reaction:

$$\left[Zn(NH_3)_4(H_2O)_2 \right]^{2+} + 2\,e^- \rightleftarrows Zn^0 + 4\,NH_3 + 2\,H_2O \quad (1)$$

The scan was reversed to the anodic direction at –1.6 V, and around –1.3 V, a crossover (E_c) was observed, associated with an electrocatalytic point. A second crossover (E_{eq}) was recorded at –1.21 V and is associated with the coexistence of the predominant redox pair under the working conditions. Peak B, recorded in the anodic region at –1.04 V, is associated with the oxidation process of the previously electrodeposited zinc.

Figure 2 shows a set of voltammograms obtained at different potential scan rates. In all cases, a rapid increase in cathodic current is observed at E < –1.28V, indicating that favorable kinetic conditions for zinc electrodeposition on the substrate surface have been reached. Furthermore, as the scan rate increases, the cathodic current associated with

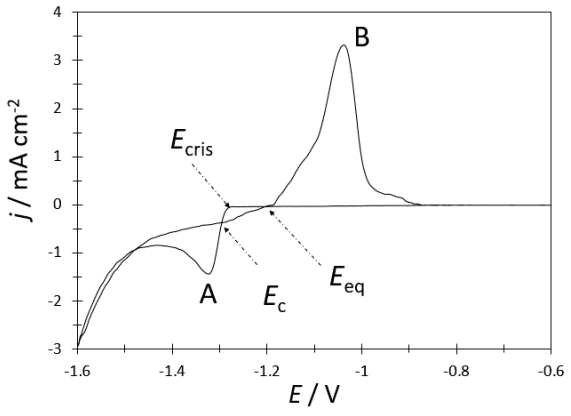

Figure 1. A cyclic voltammogram recorded from the HOPG/10^{-2} M $ZnSO_4$ + 1 M $(NH_4)_2SO_4$ system. The potential scan began at –0.600 V in the negative direction with a scan rate of 20 mV s^{-1}.

peak A shifts to more negative potentials, while peak B shifts to more positive values. This behavior suggests an increase in the system's irreversibility.[47]

To determine the limiting control of zinc electrodeposition associated with peak B, the current density corresponding to peak A was plotted against $v^{1/2}$ (where v is the scan rate), as shown in Figure 3,[48]

$$j_p = 367\, n^{3/2}\, C_0\, D^{1/2}\, v^{1/2} \quad (2)$$

A clear linear relationship between j_p and $v^{1/2}$ was observed, indicating diffusion control of the zinc electrodeposition process on the HOPG electrode. The slope's value allowed for the calculation of the diffusion coefficient, determined to be 2.6×10^{-6} cm^2 s^{-1}.

It is well established that plotting the logarithm of peak current versus the logarithm of scan rate provides detailed information about electrochemical mechanisms.[47]

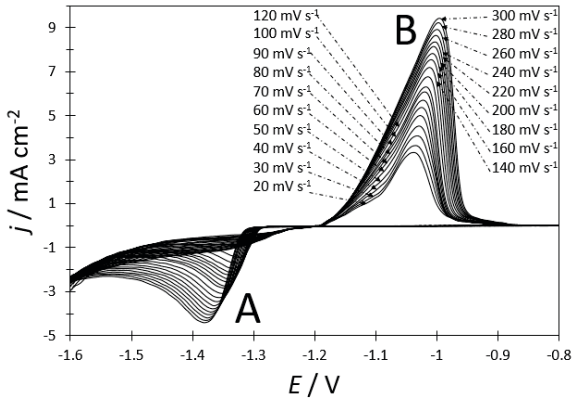

Figure 2. A set of cyclic voltammograms recorded from the HOPG/10^{-2} M $ZnSO_4$ + 1 M $(NH_4)_2SO_4$ system at different scan rates.

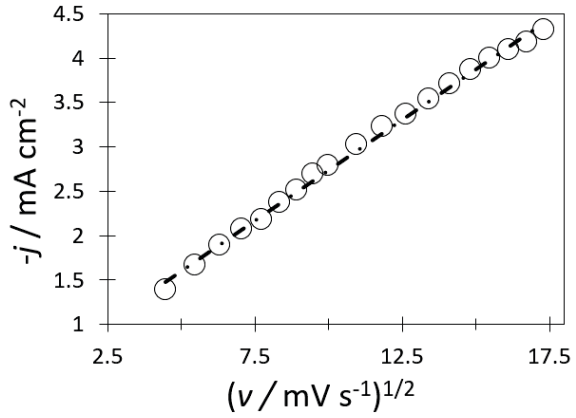

Figure 3. Plot of the experimental cathodic peak current density (j_p) as a function of the square root of the scan rate for peak A (see Figure 2). The dashed line represents the linear fit of the experimental data.

Therefore, we plotted log j_p vs. log v (see Figure 4) for cathodic peak A. The equation for peak A is $\log j_{pA} = 0.42 \log v - 2.14$. Note that the slope of the graph for cathodic peak A is close to 0.5, indicating diffusion-controlled electrochemical behavior without the influence of additional adsorption processes.[47]

Additionally, the behavior of cathodic peak potential of peak A against log v was plotted, as shown in Figure 5, revealing that E_p exhibited a linear increase with log v. The derived equation for the reduction process is $E_p = -0.0473 \log v - 1.2564$. Here it is important to consider that an irreversible process governed by diffusion can be represented by the following equation,[49]

$$E_p = \frac{2.303\, RT}{\alpha n F} \log v + c \quad (3)$$

in which R represents the gas constant, T signifies the absolute temperature in Kelvin, F denotes the Faraday

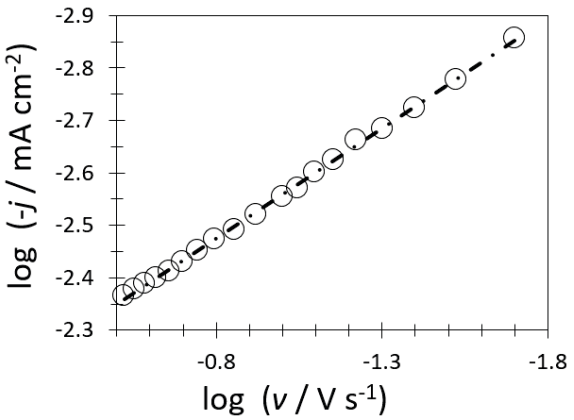

Figure 4. Plot of the log of the experimental cathodic peak current density (j_p) as a function of the log of the scan rate for peak A. The dashed line represents the linear fit of the experimental data.

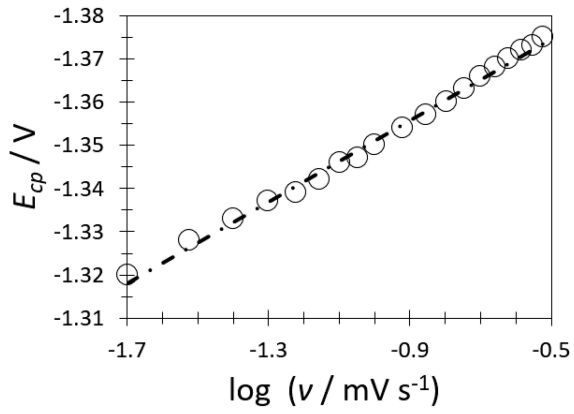

Figure 5. Plot of the cathodic peak potential of peak A vs. log v.

constant, α indicates the charge transfer coefficient, and c is a constant. Thus, from Eq. (3), the value of α for the reduction of Zn is calculated as 0.62, aligning well with values found in existing literature regarding Zn deposition on carbon substrates.[10]

Chronoamperometry

Current density transients provide valuable insights into the kinetics of the electrodeposition process.[50] In this study, chronoamperometry was used to determine the kinetic parameters related to the nucleation and growth of zinc on highly oriented pyrolytic graphite (HOPG) at pH 8. Figure 6 shows a series of current density transients recorded at various potential values using the step potential technique. Initially, a potential of –0.600 V was applied to the HOPG electrode surface, where Zn deposition had not yet begun. A subsequent negative potential step was then applied within the range of –1.29 to –1.39 V. This potential range was chosen based on the voltammetric study, starting from the potential where the Zn reduction process begins and extending to the point where the current peak appears. From Figure 6, note that each current density transient curve (j vs. t) reaches a current density maximum before approaching to the limiting diffusion current. This behavior is characteristic of three-dimensional nucleation and growth processes controlled by mass transfer.[51–53] These results, along with the voltammetric data, suggest that Zn electrodeposition onto HOPG is diffusion-controlled.

Based on the transients shown in Figure 6, nucleation can be classified as either instantaneous or progressive using the Sharifker-Hills equations.[54] To determine this, we compared the experimental transients of non-dimensional form, j^2 / j_m^2 vs t / t_m, with the theoretical curves generated from the instantaneous and progressive nucleation models, described by Eq. (4) and Eq. (5), respectively (see Figure 7).

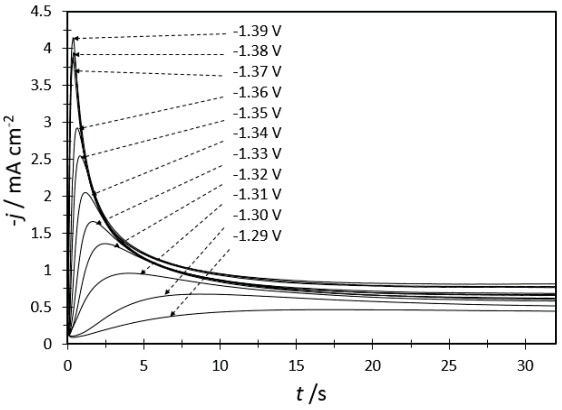

Figure 6. Current density transients obtained from the HOPG/10^{-2} M $ZnSO_4$ + 1 M $(NH_4)_2SO_4$ system.

$$\frac{j^2}{j_m^2} = 1.9542\left(\frac{t}{t_m}\right)^{-1}\left\{1-\exp\left[-2.2564\left(\frac{t}{t_m}\right)\right]\right\}^2 \quad (4)$$

$$\frac{j^2}{j_m^2} = 1.2254\left(\frac{t}{t_m}\right)^{-1}\left\{1-\exp\left[-2.3367\left(\frac{t}{t_m}\right)^2\right]\right\}^2 \quad (5)$$

It is important to note that the current density transients fall within the validity range of the model proposed by Sharifker and Hills. After reaching their maxima, the transients exhibit behavior consistent with progressive nucleation, which could lead to the formation of Zn particles of varying sizes on the HOPG surface. Additionally, it is crucial to consider that the Zn nuclei formed during electrodeposition may act as catalytic centers for the proton reduction process.[55] Therefore, the current density transients shown in Figure 6 can be explained by the following equation.[56]

$$j_{3D-PR}(t) = \left\{P_1 + P_4 t^{-1/2}\right\} \times \left\{1-\exp\left[-P_2\left[t - \frac{1-\exp(-P_3 t)}{P_3}\right]\right]\right\} \quad (6)$$

where $j_{3D-PR}(t)$ represents the current density associated with the zinc nucleation and growth process, which occurs concurrently with the proton reduction reaction on the electrode surface. In Eq. (6)

$$P_1 = z_{PR} F k_{PR}\left(\frac{2cM}{\pi\rho}\right)^{1/2} \quad (7)$$

$$P_2 = N_0 \pi\left(\frac{8\pi c}{\rho}\right)^{1/2} D \quad (8)$$

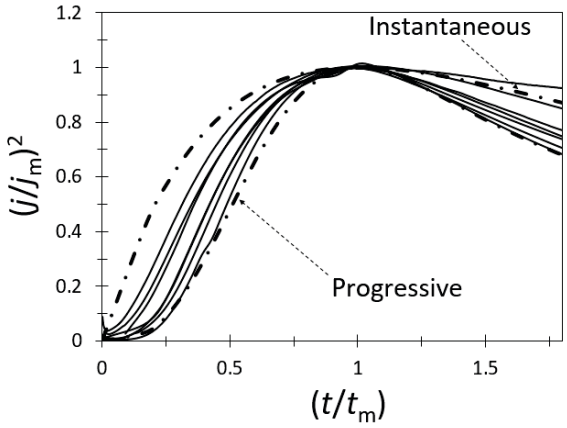

Figure 7. Non-dimensional experimental transients compared with the theoretical ones generated from equations (4) (3D instantaneous nucleation) and (5) (3D progressive nucleation).

$$P_3 = A \quad (9)$$

$$P_4 = \frac{2FD^{1/2}c}{\pi^{1/2}} \quad (10)$$

z_{PR} is the number of electrons transferred during the proton reduction reaction, and k_{PR} is the rate constant of the proton reduction process. The nucleation rate and the number of active nucleation sites are represented as A, and N_0 respectively. All the other parameters used in Eqs. (6)–(10) have their electrochemical conventional meanings. Furthermore, if we take into account the contribution of the double layer to the initial recorded current, the total current density contribution to the transient may be calculated as follows:

$$j_T = j_{dl} + j_{3D-PR} \quad (11)$$

where

$$j_{dl}(t) = k_1 e^{-k_2 t} \quad (12)$$

where $j_{dl}(t)$ is the current density for a Langmuir type adsorption process with $k_1 = k_2 Q_{dl}$ and Q_{dl} is the charge density due to the adsorption process.[57]

Figure 8 presents a comparison between the experimental current transients and the theoretical ones obtained through nonlinear fitting of the experimental data to Eq. (11). The model described by Eq. (11) accurately reproduces the behavior of all experimental transients, demonstrating its suitability for describing the system. The physical parameters extracted from the fitting process are summarized in Table 1. An increase in the nucleation rate and the number density of active sites was observed with higher applied overpotentials, indicating that the electrodeposition process becomes more favorable under these conditions. The average diffusion coefficient obtained from the fitting is 3×10^{-6} cm^2 s^{-1}, which compares well with the value obtained from voltammetric studies and with previously reported in the literature,[6,42] further supporting the reliability of the present results. Additionally, nonlinear fitting enabled the separation of current density contributions corresponding to each of the processes under study: double-layer charging, proton reduction, and nucleation and growth. For each process, the corresponding current–time curves were plotted, and the area under each curve (electric charge associated with that specific process) was quantified. The percentage contributions of each process to the total charge at different applied potentials are presented in Figure 9. As shown in Figure 9, the charge associated with double-layer charging remains approximately constant, averaging around 1.5 %. In contrast, the proton reduction process accounts for about 23.2 %, while the nucleation and growth (electrodeposition) process contributes approximately 75.3 % of the total charge. However, as the applied potential becomes more negative, the contribution from

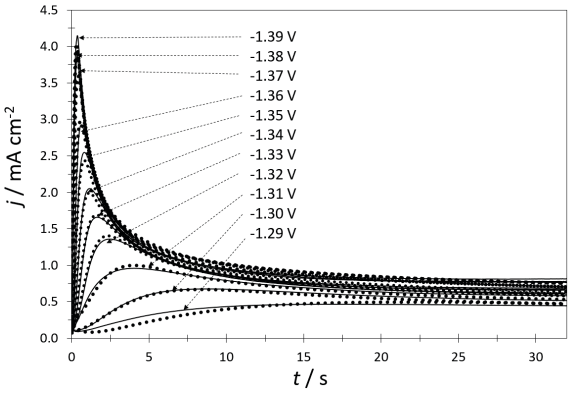

Figure 8. Comparison between the experimental current density transients (–) recorded during Zn electrodeposition obtained from the HOPG/10^{-2} M $ZnSO_4$ + 1 M $(NH_4)_2SO_4$ system. system at different applied potentials and the corresponding theoretical transient (●) generated by non-linear fitting of Eq. (11) to the experimental data.

Table 1. Potential dependence for the nucleation parameters during Zn electrodeposition on a HOPG electrode from the HOPG/10^{-2} M $ZnSO_4$ + 1 M $(NH_4)_2SO_4$ system. The values were obtained from the best-fit parameters found through the fitting process of the experimental *j*-*t* plots using Eq. (13).

E / V	A / s^{-1}	$N_0 \times 10^{-7}$ / cm^{-2}
–1.29	0.26	0.002
–1.30	0.30	1.207
–1.31	0.42	2.467
–1.32	0.40	6.230
–1.33	0.48	9.535
–1.34	0.72	12.094
–1.35	0.76	20.804
–1.36	1.68	19.558
–1.37	2.52	29.110
–1.38	2.66	37.147
–1.39	3.03	42.005

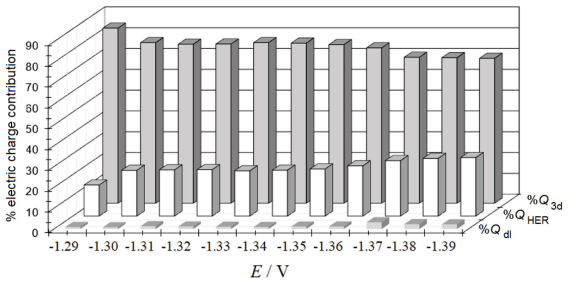

Figure 9. Percentage of electric charge contribution from the different processes at various applied potentials. Q_{dl} = charge associated with double-layer charging, Q_{HER} = charge from the proton reduction (hydrogen evolution) reaction, Q_{3D} = charge associated with the zinc electrodeposition process.

proton reduction increases, reducing the charge available for nucleation and growth. Probably, it is due to the increase in electrocatalytic activity, as shown by the increase in surface area as the electrodeposition process occurs.[58] Also, this trend suggests a competitive interaction between proton reduction and Zn nucleation/growth at more cathodic potentials, which can influence the morphology of Zn electrodeposits. Furthermore, an overall deposition efficiency of 75.3 % was achieved, which is higher than values reported in previous studies.[59]

Analysis of the Kinetical Parameters

Also, it is possible to calculate the saturation nuclear number (N_S) using Eq. (13):[54]

$$N_S = \left(\frac{AN_0}{sk'D} \right)^{1/2} \quad (13)$$

where

$$k' = \frac{4}{3}\left(\frac{8\pi c_0 M}{\rho} \right)^{1/2} \quad (14)$$

In Eq. (13), A, N_o, and D are defined as follows: A represents the nucleation rate, N_o is the number of active nucleation sites, and D is the diffusion coefficient. In Eq. (14), c_o denotes the initial concentration in the plating bath, M is the molecular weight of zinc, and ρ is the density of zinc. The values of N_s are reported in Table 2. Note that these values increase as the applied potential becomes more negative. This behavior is attributed to the increase in the nucleation rate at more negative potentials. This reduction is attributed to the depletion of concentration around the growing centers influenced by mass transfer,

Table 2. N_s values calculated from physical constants reported in Table 1 according to Eq. (13).

E / V	$N_S \times 10^{-6}$ / cm^{-2}
–1.29	0.003
–1.30	1.108
–1.31	1.718
–1.32	2.492
–1.33	3.261
–1.34	4.472
–1.35	5.895
–1.36	8.213
–1.37	13.949
–1.38	15.794
–1.39	18.284

which decreases the likelihood of nucleation occurring near existing nuclei.

Furthermore, under the principles of atomistic theory regarding electrolytic nucleation, the critical nuclei size of the Zn nucleus (n_c) was determined by considering the liner relationship between A with the applied potential, utilizing the Eq. (13).[60]

$$n_c = \left(\frac{K_B T}{z e_0} \right)\left(\frac{d \ln A}{d\eta} \right) - \alpha \quad (15)$$

where α is the transfer coefficient for Zn reduction. The plots of ln A vs η in Figure 10 exhibited a linear trend, and the critical cluster size calculated using Eq. (15) was $n_c = 0$, indicating that each atom on the surface acts as an active site. This value is similar to the number of nuclei (n_c) obtained when Zn is electrodeposited on GCE and HOPG substrates.[6]

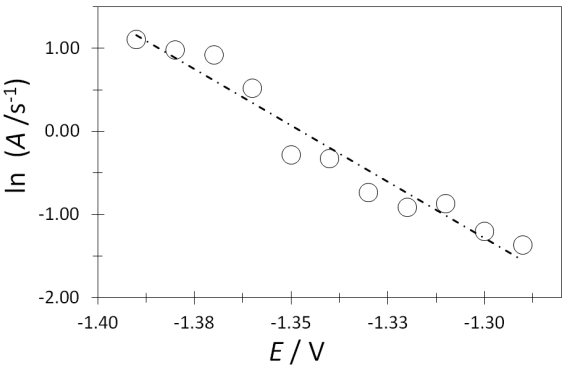

Figure 10. ln A vs E plot. The dashed straight line corresponds to the linear fit of the experimental data to Eq. (15).

Morphological Study

The morphology of the Zn deposits was examined using a JEOL 6300 scanning electron microscope (SEM). Figure 11 shows SEM images of the Zn deposits formed potentiostatically at –1.290 V and –1.370 V. Note from Figure 11 that the deposit formed at –1.290 V exhibits a homogeneous structure, while at –1.370 V the deposit shows increased roughness. This change in morphology can be attributed to the more negative potential, which is close to the hydrogen evolution reduction (HER) potential. The hydrogen bubbles generated during the electrodeposition process may interfere with the deposit formation, promoting the appearance of large clusters on the electrode surface. This phenomenon is more pronounced at more negative potentials, where hydrogen evolution is more favored. Therefore, the roughness observed at –1.370 V could be a direct result of the competition between the Zn electrodeposition process and hydrogen reduction.

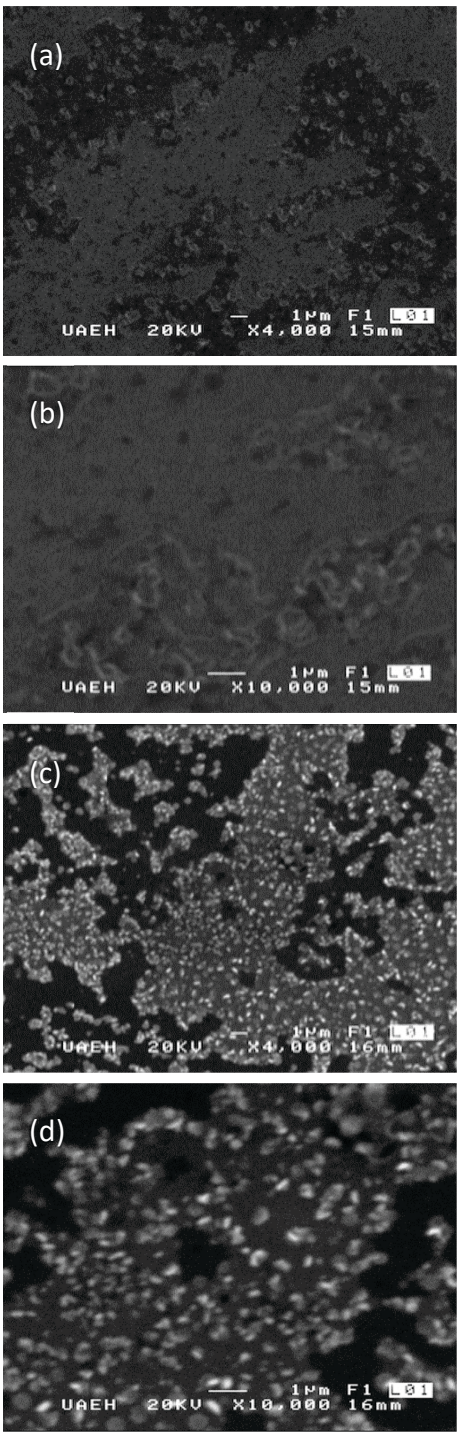

Figure 11. SEM images of the Zn electrodeposits obtained at –1.29 V (a) and (b); and at –1.39 V (c) and (d).

CONCLUSIONS

Zinc was electrodeposited onto Highly Oriented Pyrolytic Graphite (HOPG) electrodes from an aqueous alkaline solution at pH 8. Voltammetric analysis indicates that, under our experimental conditions, Zn electrodeposition is diffusion-controlled, with a charge transfer coefficient of 0.62. Nondimensional current density transients suggest the occurrence of progressive nucleation. Kinetic studies reveal that nucleation and growth parameters, such as the nucleation rate constant (A), depend on the applied potential, increasing as the potential becomes more negative. Additionally, the results suggest that hydrogen evolution at more negative potentials contributes to the formation of rough Zn electrodeposits, in contrast to the smoother deposits obtained at more positive potentials. This effect can be attributed to the competitive reduction of hydrogen at active nucleation sites, which may influence the nucleation and growth process of Zn.

REFERENCES

[1] B. Chatterjee, *Jahrb. Oberfl.* **2017**, *72,* 1–34.
[2] Z. Chen, J. Wang, H. Wu, J. Yang, Y. Wang, J. Zhang, Q. Bao, M. Wang, Z. Ma, W. Tress, et al., *Nat. Commun.* **2022**, *13*, 1–12. https://doi.org/10.1038/s41467-022-32010-y
[3] B. Ángel-Hernández, F. Hernández-Aldana, G. Pérez-Osorio, J. E. M. Gutiérrez-Arias, *Rev. Mex. Ing. Quim.* **2021**, *20*, Cat2438. https://doi.org/10.24275/rmiq/Cat2438
[4] A. I. Oliva, P. E. Martín-Várguez, I. J. González-Panzo, I. J. González-Chan, A. I. Oliva, P. E. Martín-Várguez, I. J. González-Panzo, I. J. González-Chan, *Rev. Mex. Ing. química*. **2016**, *15*, 209–220.
[5] N. Lal, K. Chawla, S. Sharma, D. K. Yadav, C. Lal, *Orient. J. Chem.* **2023**, *39*, 136–143. https://doi.org/10.13005/OJC/390116

[6] M. Granados-Neri, L. H. Mendoza-Huizar, C. H. Rios-Reyes, *Quim. Nov.* **2011**, *34*, 439–443. https://doi.org/10.1590/S0100-40422011000300014
[7] R. C. M. Salles, G. C. G. De Oliveira, S. L. Díaz, O. E. Barcia, O. R. Mattos, *Electrochim. Acta*. **2011**, *56*, 7931–7939. https://doi.org/10.1016/j.electacta.2010.12.026
[8] L. Fuller, J. Martin, Y. Ma, S. King, S. Sen, *ChemistrySelect*. **2021**, *6*, 5426–5434. https://doi.org/10.1002/slct.202101193
[9] J. R. Park, H. T. Kim, *Plat. Surf. Finish.* **1999**, *86*, 108–112.
[10] L. H. Mendoza-Huizar, C. H. Rios-Reyes, M. G. Gómez-Villegas, *J. Mex. Chem. Soc.* **2009**, *53*, 243–247.
[11] Z. Wu, X. Yuan, M. Jiang, L. Wang, Q. Huang, L. Fu, Y. Wu, *Energy and Fuels*. **2020**, *34*, 13118–13125. https://doi.org/10.1021/acs.energyfuels.0c02367
[12] N. Alias, A. A. Mohamad, *J. King Saud Univ. - Eng. Sci.* **2013**, *27*, 43–48. https://doi.org/10.1016/j.jksues.2013.03.003
[13] H. Faid, *Sigma J Eng Nat Sci.* **2016**, *37*, 1–23.
[14] J. Dundálek, I. Šnajdr, O. Libánský, J. Vrána, J. Pocedič, P. Mazúr, J. Kosek, *J. Power Sources*. **2017**, *372*, 221–226. https://doi.org/10.1016/j.jpowsour.2017.10.077
[15] D. M. Dražić, S. Hadži Jordanov, Z. Nagy, *Croat. Chem. Acta*. **1973**, *45*, 199–211.
[16] M. Amiri, D. Bélanger, *ChemElectroChem*. **2021**, *8*, 2737–2745. https://doi.org/10.1002/celc.202100541
[17] J. Lash, R. W. Herr, "Additive and alkaline zinc electroplating bath and process using same Patent (Patent # 4,366,036 issued December 28, 1982) - Justia Patents Search," **1980**, available at https://patents.justia.com/patent/4366036
[18] M. F. De Carvalho, I. A. Carlos, *Electrochim. Acta*. **2013**, *113*, 229–239. https://doi.org/10.1016/j.electacta.2013.09.136
[19] R. Ramanauskas, *Appl. Surf. Sci.* **1999**, *153*, 53–64. https://doi.org/10.1016/S0169-4332(99)00334-7
[20] H. Kim, B. N. Popov, K. S. Chen, *Corros. Sci.* **2003**, *45*, 1505–1521. https://doi.org/10.1016/S0010-938X(02)00228-7
[21] B. Veeraraghavan, B. Haran, S. P. Kumaraguru, B. Popov, *J. Electrochem. Soc.* **2003**, *150*, B131. https://doi.org/10.1149/1.1556015/XML
[22] W. McFarland, Zinc Electroplating Baths and Process. Patenet US3778359A, **1979**.
[23] K. Glaser, W. Streit, R. Fikentscher, G. Gotsmann, U.S. Patent for Zinc Electroplating Bath Patent (Patent # 4,178,217 Issued December 11, 1979) - Justia Patents Search, **1979**.
[24] C. V. Bishop, U.S. Patent for Alkaline Zinc Electroplating Bath and Additive Compositions Therefor Patent (Patent # 4,210,500 Issued July 1, 1980) - Justia Patents Search, **1980**.
[25] J. Lash, R. W. Herr, Additive and Alkaline Zinc Electroplating Bath and Process Using Same Patent (Patent # 4,366,036 Issued December 28, 1982) - Justia Patents Search, **1980**.
[26] K. Lowery, T. W. Starinshak, Acid Zinc Plating Baths and Methods for Electrodepositing Bright Zinc Deposits. Patent US4162947A, **1980**.
[27] A. J. Mohammed, M. Moats, *Metals (Basel).* **2022**, *12*, 621. https://doi.org/10.3390/MET12040621
[28] F. Rouabhia, Y. Hamlaoui, A. Meroufel, F. Pedraza, *J. Appl. Electrochem.* **2021**, *51*, 567–580. https://doi.org/10.1007/s10800-020-01517-x
[29] M. Chandran, Trans. SAEST (Society Adv. Electrochem. Sci. Technol. **2006**, 41, 35–47.
[30] Z. Zhan, Q. Zhang, S. Wang, X. Liu, Z. Sun, K. Zhang, N. Du, W. Shu, *Int. J. Electrochem. Sci.* **2021**, *16*, 210334. https://doi.org/10.20964/2021.03.24
[31] S. B. Jeon, B. K. Son, J. W. Choi, I. Son, *Coatings*. **2023**, *13*, 781. https://doi.org/10.3390/COATINGS13040781
[32] A. Keyvani, M. Yeganeh, H. Rezaeyan, *J. Mater. Eng. Perform.* **2017**, *26*, 1958–1966. https://doi.org/10.1007/s11665-017-2619-5
[33] A. El Fazazi, M. Ouakki, M. Cherkaoui, J. *Bio- Tribo-Corrosion*. **2021**, *7*, 1–22. https://doi.org/10.1007/s40735-021-00482-y
[34] H. Kancharla, G. K. Mandal, H. S. Maharana, S. S. Singh, K. Mondal, *J. Mater. Eng. Perform.* **2023**, *32*, 2993–3006.
[35] I. Ivanov, *Hydrometallurgy*. **2004**, *72*, 73–78. https://doi.org/10.1016/S0304-386X(03)00129-4
[36] H. Li, W. Jia, P. Chen, L. Wang, X. Yan, Y. Y. Yang, *Appl. Surf. Sci.* **2023**, *607*, 155111. https://doi.org/10.1016/J.APSUSC.2022.155111
[37] J. O. Bockris, Z. Nagy, D. Drazic, *J. Electrochem. Soc.* **1973**, *120*, 30. https://doi.org/10.1149/1.2403396
[38] K. Raeissi, A. Saatchi, M. A. Golozar, J. A. Szpunar, *Surf. Coatings Technol.* **2005**, *197*, 229–237. https://doi.org/10.1016/J.SURFCOAT.2004.09.024
[39] J. Torrent-Burgués, E. Guaus, *J. Appl. Electrochem.* **2007**, *37*, 643–651. https://doi.org/10.1007/s10800-007-9296-2
[40] M. Granados Neri, L. H. Mendoza Huizar, in *ECS Trans.*, Vol. 29, **2010**.
[41] M. Plata, S. Olvera, C. Ramírez-Rodríguez, H. Dorantes-Rosales, E. M. Arce-Estrada, *ECS Trans.* **2007**, *3*, 25–33. https://doi.org/10.1149/1.2721514/XML

[42] A. E. Alvarez, D. R. Salinas, *J. Electroanal. Chem.* **2004**, *566*, 393–400. https://doi.org/10.1016/J.JELECHEM.2003.11.051
[43] P. J. Sonneveld, W. Visscher, E. Barendrecht, *Electrochim. Acta*. **1992**, *37*, 115–9405. https://doi.org/10.1016/0013
[44] I. Kryshtop, N. Yurchenko, V. Trofimenko, *ECS Trans.* **2008**, *13*, 65–70. https://doi.org/10.1149/1.3005184/XML
[45] J. Yu, H. Yang, X. Ai, Y. Chen, *Russ. J. Electrochem.* **2002**, *38*, 321–325. https://doi.org/10.1023/A:1014751327614
[46] G. Trejo, R. Ortega B., Y. Meas, P. Ozil, E. Chainet, B. Nguyen, *J. Electrochem. Soc.* **1998**, *145*, 4090–4097. https://doi.org/10.1149/1.1838919/XML
[47] A. J. Bard, L. R. Faulker, *Métodos Electroquímicos. Fundamentos y Aplicaciones*, 2a ed., Wiley Nueva York **2001**.
[48] T. Berzins, P. Delahay, *J. Am. Chem. Soc.* **1953**, *75*, 555–559. https://doi.org/10.1021/ja01099a013
[49] E. Laviron, *J. Electroanal. Chem.* **1979**, *101*, 19–28. https://doi.org/10.1016/S0022-0728(79)80075-3
[50] L. H. Mendoza-Huizar, G. A. Álvarez Romero, M. E. Paez Hernández, M. Rivera, *Croat. Chem. Acta*. **2024**, *97*, 119–129. https://doi.org/10.5562/cca4122
[51] M. Sluyters-Rehbach, J. H. O. J. Wijenberg, E. Bosco, J. H. Sluyters, *J. Electroanal. Chem. Interfacial Electrochem.* **1987**, *236*, 1–20. https://doi.org/10.1016/0022-0728(87)88014-2
[52] B. R. Scharifker, J. Mostany, M. Palomar-Pardavé, I. González, *J. Electrochem. Soc.* **1999**, *146*, 1005. https://doi.org/10.1149/1.1391713
[53] L. Heerman, A. Tarallo, *J. Electroanal. Chem.* **1999**, *470*, 70–76. https://doi.org/10.1016/S0022-0728(99)00221-1
[54] B. Scharifker, G. Hills, *Electrochim. Acta*. **1983**, *28*, 879–889. https://doi.org/10.1016/0013-4686(83)85163-9
[55] M. Rezaei, S. H. Tabaian, D. F. Haghshenas, *Electrochim. Acta*. **2013**, *87*, 381–387. https://doi.org/10.1016/j.electacta.2012.09.092
[56] M. Palomar-Pardavé, B. R. Scharifker, E. M. Arce, M. Romero-Romo, *Electrochim. Acta*. **2005**, *50*, 4736–4745. https://doi.org/10.1016/j.electacta.2005.03.004
[57] M. H. Hölzle, U. Retter, D. M. Kolb, *J. Electroanal. Chem.* **1994**, *371*, 101–109. https://doi.org/10.1016/0022-0728(93)03235-H
[58] Z. Grubač, A. Sesar, *Croat. Chem. Acta*. **2017**, *90*, 273–280.
[59] https://doi.org/10.5562/cca3174
[60] C. Müller, M. Sarret, M. Benballa, *J. Electroanal. Chem.* **2002**, *519*, 85–92. https://doi.org/10.1016/S0022-0728(01)00725-2
[61] A. Milchev, *Electrocrystallization. Fundamentals of Nucleation and Growth*, 1st ed., Vol. 1, Kluwer Academic Publishers, Dordrecht **2002**.